molecular pharmaceutics

pubs.acs.org/molecularpharmaceutics Article

Cell Type-Dependent Specificity and Anti-Inflammatory Effects of Charge-Reversible MSNs-COS-CMC for Targeted Drug Delivery in Cervical Carcinoma

Lan Cui, Xiayi Feng, Wentao Liu,* Hao Liu,* Qian Qin, Shuangxia Wu, Suqin He, Xinchang Pang, Dong Men, and Chengshen Zhu*

Cite This: https://dx.doi.org/10.1021/acs.molpharmaceut.0c00004 Read Online

ABSTRACT: The surface charge of nanocarriers inevitably affects drug delivery efficiency; however, the cancer cell specificity, anti-inflammatory effects, and charge-reversal points remain to be further addressed in biomedical applications. The aim of this study was to comprehensively assess the cancer cell specificity of DOX-loaded mesoporous silica-chitosan oligosaccharide-carboxymethyl chitosan nanoparticles (DOX@MSNs-COS-CMC) in MCF-7 and HeLa cells, inhibit the production of inflammatory cytokines, and improve the drug accumulation in the tumor site. Intracellular results reveal that the retention time prolonged to 48 h in both HeLa and MCF-7 cells at pH 7.4. However, DOX@MSNs-COS-CMC exhibited a cell type-dependent cytotoxicity and enhanced intracellular uptake in HeLa cells at pH 6.5, due to the clathrin-mediated endocytosis and macropinocytosis in HeLa cells in comparison with the vesicular transport in MCF-7 cells. Moreover, Pearson's correlation coefficient value significantly decreased to 0.25 after 8 h, prompting endosomal escape and drug delivery into the HeLa nucleus. After the treatment of MSNs-COS-CMC at 200 μg/mL, the inflammatory cytokines IL-6 and TNF-α level decreased by 70% and 80%, respectively. Tumor inhibition of DOX@MSNs-COS-CMC was 0.4 times higher than free DOX, alleviating cardiotoxicity and inflammation in the HeLa xenograft tumor model. Charge-reversible DOX@MSNs-COS-CMC could be a possible candidate for clinical therapy of cervical carcinoma.

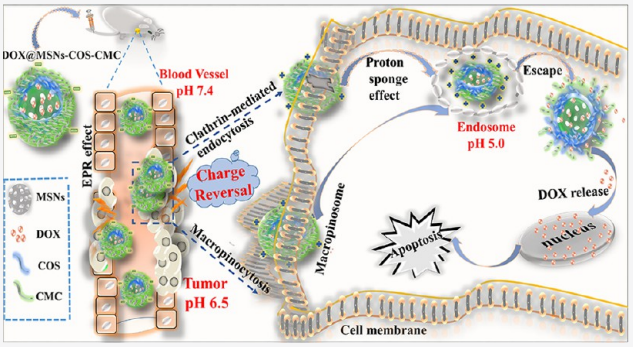

KEYWORDS: *cell specificity, anti-inflammatory, charge reversal, chitosan oligosaccharide, cervical carcinoma*

1. INTRODUCTION

Chemotherapeutic drugs lack specificity to cancerous and normal tissues,[1] inevitably inducing adverse effects and systemic toxicity. Nowadays, stimuli-responsive nanoparticles have been considered as a promising vehicle for improving tumor specificity and cellular uptake via the enhanced permeability and retention effect.[2] Among the internal stimulus (e.g., pH, redox, and enzymes) and external triggers (e.g., light, thermal energy, and ultrasound), pH-stimulus has been an effective alternative since the pH values in tumor tissues (pH 6.5−6.9) and endo/lysosomes (pH 5.0−5.5) are obviously lower than normal physiological environment (pH 7.4). However, nanoparticles remain need to overcome the physiological and biological barriers in the drug delivery system, it is highly desirable to design more intelligent nanoparticles to prompt effective endocytosis and endosomal escape, overcome lysosomal degradation, improve cancer cell specificity, and control drug release in vivo.[3]

The surface charge of materials is an indispensable factor in the comprehensive investigation of the drug delivery system. Recently, pH-induced charge-reversible nanoparticles have exhibited remarkable superiority in prompting cellular uptake and tumor accumulation.[4−6] Notably, the negative charge endows nanoparticles with a higher stability and longer blood circulation time,[7,8] through avoiding nonspecific interaction with serum proteins and reducing phagocytosis of the reticuloendothelial system.[9,10] The positive charge facilitates the adsorption-mediated endocytosis and the cell membrane rupture through the proton sponge mechanism, which favors nanoparticles that escape from the lysosomal trap.[11−14] Recently, our group has designed a charge-reversible nanocarrier, DOX@MSNs-CS-CMC,[15] via the ion-cross-linking and self-assembly among mesoporous silica nanoparticles (MSNs),

Received: January 2, 2020
Revised: March 29, 2020
Accepted: March 30, 2020
Published: March 30, 2020

Scheme 1. Schematic Illustration of Charge-Conversion and Extracellular DOX Release of DOX@MSNs-COS-CMC by the pH Trigger

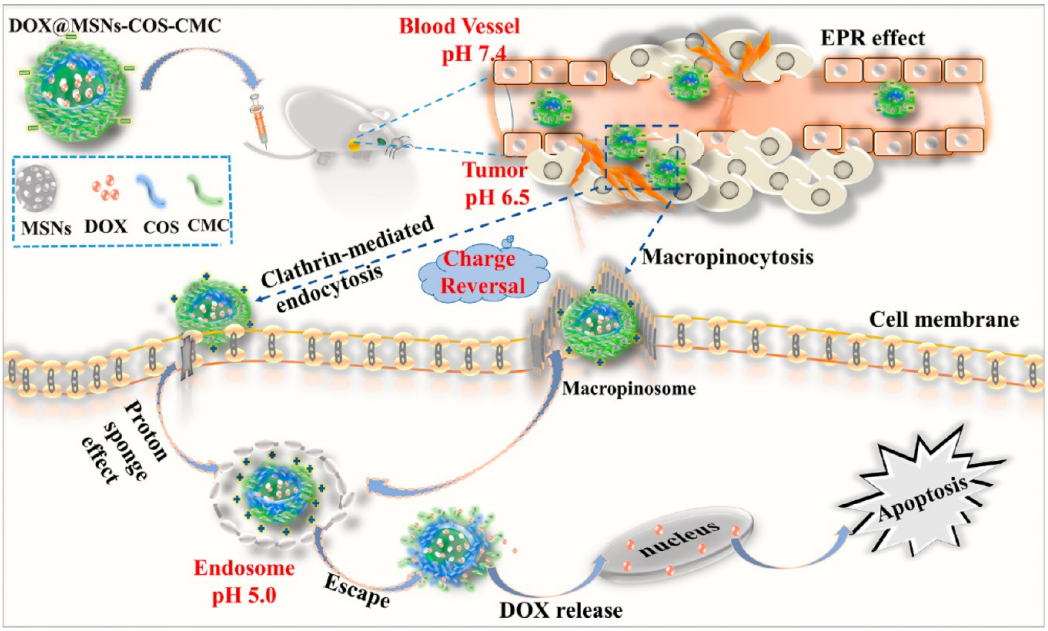

chitosan (CS), carboxymethyl chitosan (CMC), and doxorubicin hydrochloride (DOX), due to the tunable pore structure of MSNs[16,17] and the excellent biocompatibility of CMC.[18−20] Despite the potential to reduce the side effects of chemotherapeutic drugs, the anti-inflammatory effects, cell type-dependent specificity, charge-reversal points, biocompatibility, and biodegradability are key to the development of efficient nanocarriers.[21−23]

Cervicitis is an inflammatory disease in women of reproductive age. Lipopolysaccharide (LPS) is a major constituent of the outer membrane of Gram-negative bacteria; it has been reported as an effective activator to induce the pro-inflammatory cytokines release in human cervical cell lines.[24,25] In addition, the inflammatory microenvironment is prone to induce tumor transformation and progression, angiogenesis, and metastasis.[25] Chitosan oligosaccharide (COS) has been investigated in the drug-induced renal failure, which might be used as an alternative in antioxidant and anti-inflammatory treatment.[26] The purpose of this study was to enhance the therapeutic effect on cervical carcinoma via assessing the cell specificity of DOX@MSNs-COS-CMC in MCF-7 and HeLa cells, anti-inflammatory effects, and tumor accumulation.

As shown in Scheme 1, charge-reversible DOX@MSNs-COS-CMC were in stepwise-response to the tumor extracellular microenvironment and further promoted drug delivery into the nucleus and induced apoptosis of HeLa cells via the protonation/deprotonation effects. The cancer cell-type specificity of DOX@MSNs-COS-CMC was investigated by evaluating the toxicity, intracellular distribution, endosomal escape, and endocytosis mechanism in both MCF-7 and HeLa cells. In addition, anti-inflammation was authenticated by reducing the production of inflammatory cytokines of tumor necrosis factor-alpha (TNF-α) and interleukin 6 (IL-6) in LPS-induced HeLa cells. The in vivo therapeutic efficacy and histopathological examination were also investigated in the HeLa xenograft tumor model. Therefore, the specific endocytosis, anti-inflammatory activity, and significant anti-tumor efficacy of charge-reversal DOX@MSNs-COS-CMC would provide a potential application for cervical carcinoma therapy.

2. EXPERIMENTAL SECTION

2.1. Materials. Tetraethyl orthosilicate, doxorubicin hydrochloride (DOX), chitosan (M_w = 200 kDa), sodium tripolyphosphate (TPP), chlorpromazine, amiloride, nocodazole, and genistein were purchased from Aladdin Chemistry Co., Ltd., China. Chitosan oligosaccharide (COS, M_w = 3 kDa) was obtained from Golden-Shell Biochemical Co., Ltd., China. Cell counter kit-8 (CCK-8) was purchased from Dojindo Laboratories, Japan. LysoTracker Green DND-26 and Hoechst 33342 were purchased from the Beyotime Institute of Biotechnology, China. Lipopolysaccharide (LPS) was purchased from Macklin Biochemical Co., Ltd.

2.2. Cell Culture and Animals. The human breast cancer cells (MCF-7 cells) and human cervical squamous carcinoma cells (HeLa cells) were cultivated in Dulbecco's modified Eagle medium containing 10% fetal bovine serum, 100 U/mL penicillin, and 100 μg/mL streptomycin. The pH of the culture medium was adjusted to 7.4 and 6.5 by 0.1 mol/L HCl, respectively.[27]

The female BALB/c nude mice (5−6 weeks old, 18 ± 2 g) were supplied by the Institute of Virology, Chinese Academy of Sciences, and fed in a specific pathogen-free environment at 20 °C for 1 week prior to being used. All animal experiments were approved and performed from an animal protocol (WIVA20201802) in accordance with the guidelines of the animal care and ethics committee of Hubei province. HeLa cancer cells (10^6 cells) were subcutaneously implanted in the right flank of nude mice to establish a xenograft tumor model.[13,28,29]

2.3. Synthesis of DOX@MSNs-COS-CMC. DOX@MSNs-COS-CMC were prepared according to our previous research[15] via the ion-cross-linking and self-assembly among the mesoporous silica nanoparticles (MSNs), sodium tripolyphosphate (TPP), chitosan oligosaccharide (COS), and carboxymethyl chitosan (CMC) to deliver doxorubicin

https://dx.doi.org/10.1021/acs.molpharmaceut.0c00004
Mol. Pharmaceutics XXXX, XXX, XXX−XXX

hydrochloride (DOX). Briefly, DOX (5 mg) and MSNs (10 mg) were mixed in phosphate buffer under magnetic stirring for 48 h in the dark. Subsequently, 0.25 mg/mL TPP was injected dropwise and incubated at 55 °C for 0.5 h. Then, 15 mL of 1 mg/mL COS and 20 mL of 1 mg/mL CMC were sequentially added and reacted for another 2 h. Finally, DOX@MSNs-COS-CMC were obtained after centrifugation and freeze-drying.

The ζ potential and size diameter were estimated by a Zetasizer Nano ZS90, Malvern Instruments Ltd., U.K. Nanoparticles were diluted in phosphate buffer solution at a concentration of 1 mg/mL; then 1.5 mL of samples was collected at predetermined time intervals to measure the intensity-averaged particle size and ζ potential changes. The microstructure and aggregation states were observed by the Nano-inXider Vertical SAXS/WAXS System, Xenocs, France. The morphology was conducted by a transmission electron microscope (TEM, Hitachi-HT7700, Hitachi Ltd., Japan). The specific surface area and pore size distribution were calculated by a surface area analyzer (BK112T, JWGB Sci.&Tech., Peking, China).

2.4. In Vitro Drug Release and Cytotoxicity. DOX-loaded nanoparticles were immersed in PBS solution, added into the dialysis bag, and incubated under constant shaking at 100 rpm and 37 °C for 72 h. The cumulative release rate was determined by an ultraviolet spectrophotometer.

The cytotoxicity of DOX-loaded nanoparticles was quantified by a CCK-8 assay. MCF-7 and HeLa cells were seeded at the density of 1×10^4 cells/well and cultured at 37 °C for 24 h. Subsequently, cells were treated with (DOX: 0−12.5 μg/mL) at pH 7.4 and 6.5. After incubation of 24 and 48 h, the CCK-8 solution was then added in the well and incubated for 3 h. The absorption at 450 nm was measured with a multimode plate reader.

2.5. Intracellular Uptake Assays in MCF-7 and HeLa Cells. The intracellular biodistribution of DOX@MSNs-COS-CMC was observed by a confocal laser scanning microscope (CLSM). MCF-7 and HeLa cells were cultured at a density of 1×10^5 cells/dish. After 24 h of incubation, cells were treated with DOX-loaded nanoparticles (DOX, 2 μg/mL) and incubated at pH 7.4 and 6.5. After the paraformaldehyde fixation and Hoechst staining, the fluorescence of cancer cells was observed to evaluate intracellular uptake.

The quantitative analysis of DOX fluorescence in MCF-7 and HeLa cells was measured by flow cytometry (BD LSRFortessa, USA). Cells were cultured at the density of 2×10^5 cells/well. After treatment of DOX-loaded nanoparticles (DOX: 2 μg/mL) at pH 7.4 and 6.5, cancer cells were digested with trypsin, centrifuged, washed, and resuspended to measure the fluorescence intensity.

2.6. Endocytic Pathway in MCF-7 and HeLa cells. Chlorpromazine, amiloride, nocodazole, and genistein were used as endocytic inhibitors to interfere with MCF-7 and HeLa cells.[30] After 6 h incubation, the cytotoxicity of inhibitors was measured by CCK-8 assay. Then concentrations of inhibitors were determined for the following endocytic studies when the minimum cell viability reached 90%.

MCF-7 and HeLa cells were cultured at the density of 2×10^5 cells/well for 24 h. The cells were then pretreated with chlorpromazine hydrochloride (4 μg/mL), amiloride hydrochloride (100 μg/mL), nocodazole (0.5 μg/mL), and genistein (60 μg/mL), respectively. After pharmacological inhibition for 1 h, cells were incubated with DOX@MSNs-COS-CMC (DOX: 2 μg/mL) at pH 6.5 for another 5 h. Then the cells were collected and resuspended in PBS buffer for the measurement of flow cytometry.

2.7. Subcellular Localization in HeLa Cells. HeLa cells were cultured at the density of 1×10^5 cells/dish for 24 h. Then HeLa cells were treated with free DOX, DOX@MSNs, and DOX@MSNs-COS-CMC (DOX: 2 μg/mL) to determine the endosomal escape at pH 6.5. After incubation of 1, 3, and 8 h, the endo/lysosomes and nucleus were stained with LysoTracker Green (30 min) and Hoechst (5 min), respectively. Then the cells were observed by a confocal laser scanning microscope.

2.8. Anti-Inflammatory Assay in HeLa Cells. HeLa cells were seeded in 24-well plates at a density of 1×10^6 cells/well and cultured at 37 °C for 24 h. Then the cells were stimulated with LPS (10 μg/mL) for 24 h, followed by treatments with different concentrations of MSNs and MSNs-COS-CMC. Cells without stimulation were used as the negative control. At the end of incubation, culture supernatants were collected to determine the cytokine concentration of tumor necrosis factor-alpha (TNF-α) and interleukin 6 (IL-6) using the human cytokine enzyme-linked immunosorbent assay (ELISA) kits (eBioscience).[24,25]

2.9. Biodistribution Evaluation in the HeLa Xenograft Tumor Model. The tumor-bearing mice were randomized into four groups (n = 3) and administrated with DOX-loaded nanoparticles at an identical dosage of 5 mg/kg through intravenous injection, when the tumor approximately reached about 300 mm^3 in volume. The biodistribution of DOX in mice was investigated via the treatment of intraperitoneal anesthesia at the predetermined time points (3, 7, 12, and 24 h). Then the mice were euthanized and sacrificed at 12 and 24 h. The tumor tissue and major organs (heart, liver, spleen, lung, and kidney) were harvested to analyze the DOX biodistribution using the IVIS system and the Maestro CRi software at the optimal wavelength (the excitation and emission filter were 455 and 490 nm).

2.10. In Vivo Antitumor Activity and Histological Examination. The tumor-bearing mice were randomly divided into four groups (n = 3) when the tumor volume approximately reached 100 mm^3; then the mice were treated with saline solution, free DOX, DOX@MSNs, and DOX@MSNs-COS-CMC (DOX dosage: 5 mg/kg) via tail vein every 2 days for 15 days. Tumor volume was calculated by the following formula: $V = \text{width}^2 \times \text{length}/2$.

Histological examinations were also utilized to evaluate the systemic toxicity of DOX in the tumor-bearing mouse. Tumor tissues and main organs, including the heart, liver, spleen, lung, and kidney, were harvested and stained with hematoxylin and eosin (H&E). The terminal deoxynucleotidyl transferase-mediated dUTP nick end labeling (TUNEL) assay was conducted to analyze the apoptosis of tumor tissue. Positive TUNEL staining was visualized by optical microscopy, the TUNEL positive ratio was analyzed by the ImageJ software, and the apoptotic index was formulated as the ratio of apoptotic cells number to the total tumor cell number in each microscopic field (n = 10).[31] Tumors and major organs were fixed by 4% paraformaldehyde, embedded in paraffin, and sectioned with 4 μm thickness. Then the stained slices were observed by an optical microscope (Chirascan-SF, Thermo & 3DHISTECH, USA) at 20× magnifications.

2.11. Statistical Analysis. Experiments were carried out at least three times. The data were expressed as the mean ±

https://dx.doi.org/10.1021/acs.molpharmaceut.0c00004
Mol. Pharmaceutics XXXX, XXX, XXX−XXX

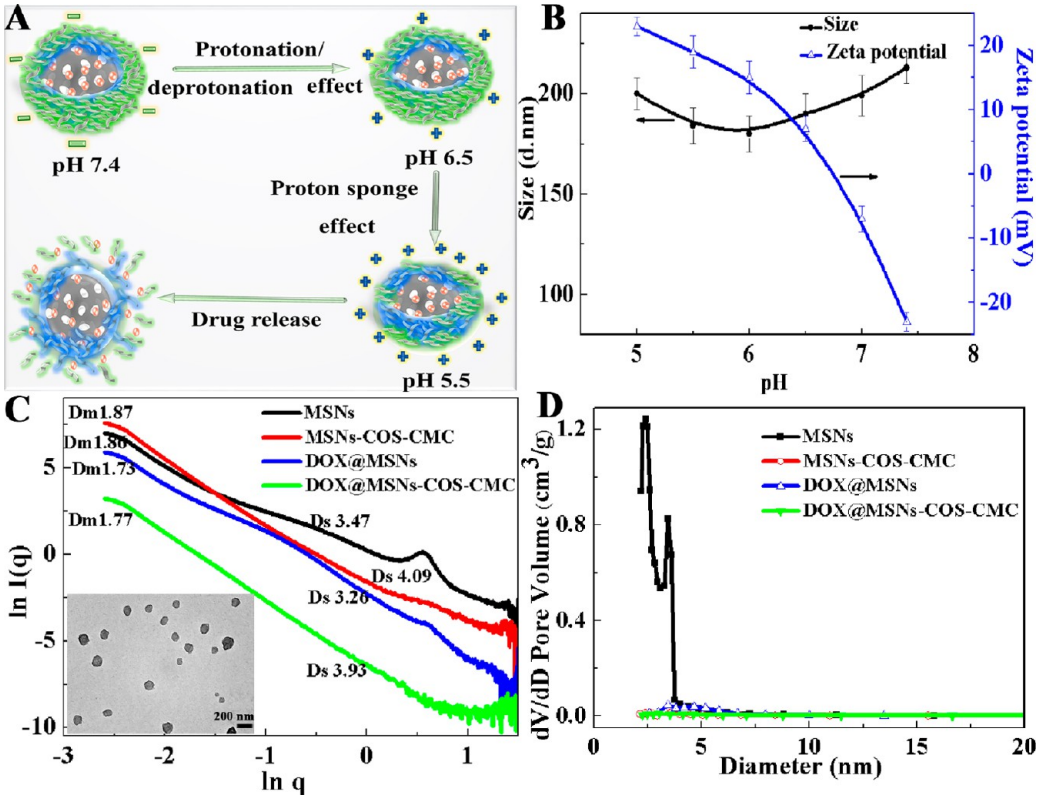

Figure 1. Characterizations of DOX@MSNs-COS-CMC. (A) Schematic illustration of charge reversal at different pH values. (B) Intensity-averaged particle size and ζ potential at different pH values. (C) ln $I(q)$ versus ln q profile by SAXS analysis. The inside figure represents the TEM image of DOX@MSNs-COS-CMC. (D) Pore size distribution curve.

standard deviation. Student's t test and one-way ANOVA were used to analyze the statistical significance using Statistical Program for Social Sciences (SPSS) software. * and ** mean $P < 0.05$ and $P < 0.01$, indicating that the results are of statistical significance and extremely statistical significance, respectively.

3. RESULTS AND DISCUSSION

3.1. Charge Reversal and Drug Release Mechanism of DOX@MSNs-COS-CMC. Charge reversal of DOX@MSNs-COS-CMC (Figure 1A,B) was realized at a weight ratio of DOX, MSNs, TPP, COS, and CMC for 1:2:0.5:3:4, in view of the protonated/deprotonated carboxyl and amino groups of CMC (pK_a 3.0−4.0, the percentage of free amino groups is 60%), COS (pK_a 6.5), and DOX (pK_a 8.3). The result elucidates that negative charge nanoparticles at pH 7.4 may prolong the lifetime during blood circulation. Moreover, nanoparticles with a smaller size would improve the deep tumor penetration.[32] DOX@MSNs-COS-CMC was less than 150 nm at pH 5.5; the changes of core−shell structure, particle size, chemical block lengths, stability, and density would have the potential to promote the tumor penetration.

SAXS results (Figure 1C and Figure S1A) show that two Bragg peaks at q values of 1.71 and 3.93 nm^{-1} are ascribed to the d_{100} and d_{200} reflections.[33,34] However, the intensity of diffraction peaks decreased, and the values of mass fractals (Dm) and surface fractals (Ds) increased after surface modification, indicating that the COS-CMC shell promoted the densification of mesopores structures and led to some distortions at the periphery of MSNs. The WAXS pattern (Figure S1B) shows the amorphous structure of MSNs at around 22°, the (020) and (110) planes of chitosan nearby 12.8° and 20.8°, respectively.[35] The crystalline diffraction peaks and BJH adsorption volume (Figure 1D) of DOX@MSNs-COS-CMC significantly decreased, confirming that DOX was encapsulated in the pores of MSNs and COS-CMC shell via hydrogen bond and ionic cross-linking interaction.

DOX@MSNs-COS-CMC owned a higher encapsulation efficiency (80%) due to the ionic cross-linking of DOX and COS-CMC shell. In addition, DOX@MSNs-COS-CMC exhibited a relatively desirable stability; the particle size retained almost unchanged at pH 7.4 (Figure S2A). However, the particle size gradually increased and then slightly reduced over time at pH 5.5. The results might be ascribed to the exposure of the cationic shell and the corrosion of the loose segment.[13]

Compared with DOX@MSNs, DOX@MSNs-COS-CMC exhibited a significant pH-dependent drug release (Figure S2B), which is attributed to the pH-triggered charge reversal. The drug release rates (28% and 36%) of DOX@MSNs-COS-CMC at pH 6.5 and 5.5 were 4.6 and 6.1 times higher than the release at pH 7.4 after 72 h, respectively. The kinetics models of drug release for DOX@MSNs-COS-CMC were shown in Table S1; it could be found that the Ritger−Peppas model was the best fitting model by comparing the correlation coefficient (R^2). The diffusion exponents at pH 7.4 were equal to 0.33, indicating a Fick diffusion. Whereas the diffusion exponents at pH 6.5 and 5.5 were 0.62 and 0.57, respectively, indicating a non-Fick diffusion. The sustained drug delivery system was a relatively complicated matrix type involving diffusion, swelling, and corrosion.[36] Thus, DOX@MSNs-COS-CMC has the potential to avoid frequent drug administration.

https://dx.doi.org/10.1021/acs.molpharmaceut.0c00004
Mol. Pharmaceutics XXXX, XXX, XXX−XXX

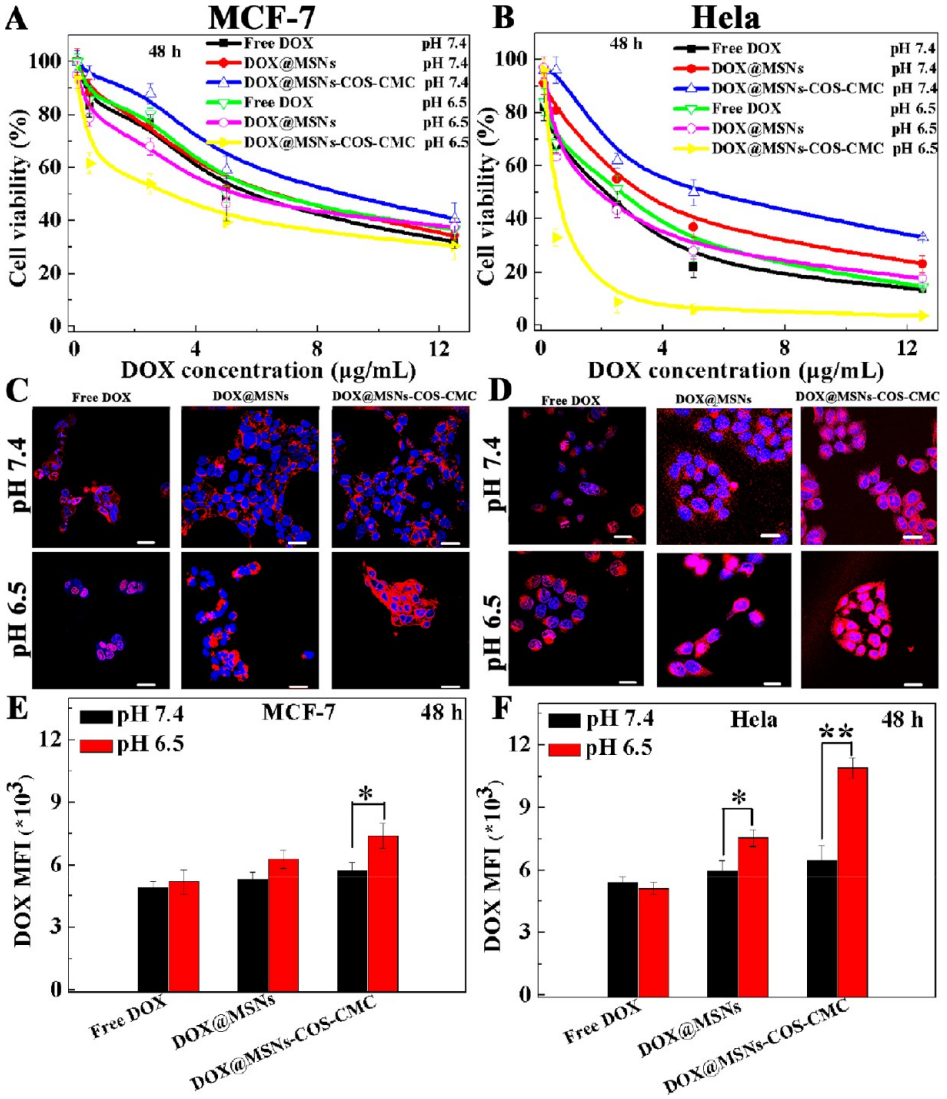

Figure 2. Cytotoxicity and intracellular uptake of drug-loaded nanoparticles in MCF-7 and HeLa cells after 48 h. (A, B) In vitro viability of MCF-7 and HeLa cells after treatments of free DOX, DOX@MSNs, and DOX@MSNs-COS-CMC at a concentration ranging from 0.1 to 12.5 μg/mL (n = 5). (C, D) CLSM images of MCF-7 and HeLa cells incubated with free DOX, DOX@MSNs, and DOX@MSNs-COS-CMC at pH 7.4 and 6.5 (DOX, 2 μg/mL; scale bar, 20 μm). Cell nuclei were stained with Hoechst (blue). (E, F) The mean fluorescence intensity (MFI) of DOX (DOX: 2 μg/mL). Data were presented as the mean value ± standard deviation (n = 3). The statistical significance was analyzed by Student's t test and one-way ANOVA using SPSS software; * means $P < 0.05$, and ** means $P < 0.01$.

3.2. Cell Type-Dependent Cytotoxicity and Intracellular Uptake in MCF-7 and HeLa Cells. The cell viability of blank nanoparticles was around 85%, showing a good biocompatibility (Figure S3A,B). Time- and dosage-dependent cytotoxicities were clearly observed in both MCF-7 and HeLa cells (Figure 2A,B and Figure S3C,D). However, the dosage-dependent cytotoxicity of DOX@MSNs-COS-CMC was significantly higher in HeLa cells than that in MCF-7 cells. It may be attributed to the specific endocytosis mechanism;[30] in addition, HeLa cells may be highly acid-sensitive due to the clathrin-mediated endocytosis and micropinocytosis, and MCF-7 cells may be slightly acid-sensitive due to the vesicular transport. Moreover, the cytotoxicity of DOX@MSNs-COS-CMC in HeLa cells at pH 6.5 was significantly higher than the toxicity at pH 7.4. As shown in Table S2, the half-maximal inhibitory concentration (IC_{50}) of DOX@MSNs-COS-CMC was 5.8 and 0.6 μg/mL at pH 7.4 and 6.5, respectively, whereas the IC_{50} of free DOX was 2.6 μg/mL at pH 6.5. Results indicate that the surface charge reversal could improve cell-type specificity, cytotoxicity, and DOX release in tumor tissues at pH 6.5.

Similar phenomena were observed from the CLSM images and flow cytometry analysis. Figure 2C,D and Figure S4 show that the DOX fluorescence of DOX@MSNs-COS-CMC was mainly accumulated in the cytoplasm but slightly distributed within the nucleus of both MCF-7 and HeLa cells at pH 7.4. However, DOX was burst into release and transferred to the perinuclear region of HeLa cells at pH 6.5. Moreover, the mean fluorescence intensity (MFI) of DOX in DOX@MSNs-COS-CMC was significantly increased in HeLa cells at an acidic microenvironment. The MFI of DOX@MSNs-COS-CMC in HeLa cells was 2.1-fold in comparison with free DOX at pH 6.5 after 48 h, whereas the difference of MFI in MCF-7 cells was 1.4-fold. Results demonstrate that the pH-responsive and charge-reversal DOX@MSNs-COS-CMC could achieve

https://dx.doi.org/10.1021/acs.molpharmaceut.0c00004
Mol. Pharmaceutics XXXX, XXX, XXX−XXX

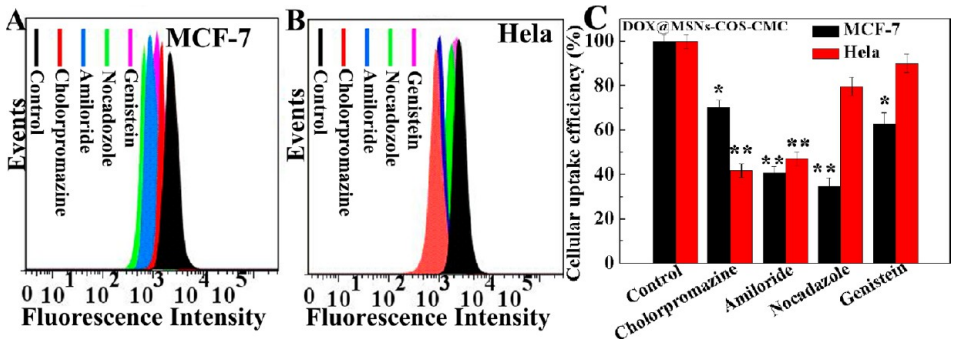

Figure 3. Endocytosis of DOX@MSNs-COS-CMC in MCF-7 and HeLa cells at pH 6.5. The internalized DOX signals in (A) MCF-7 and (B) HeLa cells by flow cytometry. (C) Effect of endocytic inhibitors on the cellular uptake efficiency. Data were presented as the mean value ± standard deviation ($n = 3$). The statistical significance was analyzed by Student's t test and one-way ANOVA using SPSS software; * means $P < 0.05$, and ** means $P < 0.01$, compared with the control group. MCF-7 and HeLa cells were preincubated with 4 μg/mL chlorpromazine hydrochloride, 100 μg/mL amiloride hydrochloride, 0.5 μg/mL nocodazole, and 60 μg/mL genistein for 1 h, respectively, followed by coincubation with DOX@MSNs-COS-CMC (DOX: 2 μg/mL) at pH 6.5 for another 5 h.

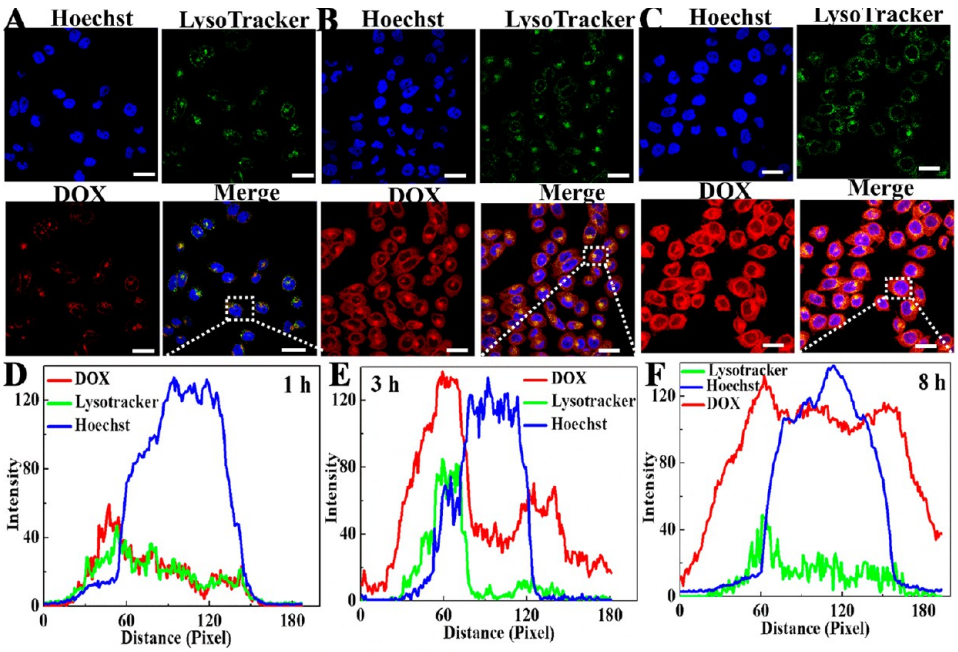

Figure 4. Endosomal escape of DOX@MSNs-COS-CMC in HeLa cells at pH 6.5 for different time courses. (A–C) Confocal microscopic images of intracellular trafficking. HeLa cells were treated with DOX@MSNs-COS-CMC for 1, 3, and 8 h, and then the endo/lysosomes and nucleus were stained with LysoTracker Green (30 min) and Hoechst (5 min), respectively. (C, D) Pixel intensity profiles to analyze localization of nanoparticles and lysosome (DOX, 2 μg/mL; scale bar, 20 μm).

cell type-dependent uptake and on-demand tumor-targeting release and possess superior DOX delivery efficacy.

The intracellular drug release from DOX@MSNs-COS-CMC was in line with higher antitumor activity and extensively shorten the time of drug delivery to the HeLa nucleus at pH 6.5, which is attributed to the charge reversal that facilitates clathrin-mediated endocytosis and micropinocytosis and the endosomal escape[13] via the interaction with the endosomal membrane and trigger the diffusion of drugs to the perinuclear region. The cell-type specificity of charge-reversible DOX@MSNs-COS-CMC would be carefully evaluated via the investigation of the endocytosis mechanism and endosomal escape in MCF-7 and HeLa cells.

3.3. Cell Type-Dependent Endocytosis in MCF-7 and HeLa cells. Chlorpromazine, amiloride, nocodazole, and genistein were used as endocytic inhibitors to interfere with the clathrin-mediated endocytosis, macropinocytosis, vesicular transport, and caveolin-mediated endocytosis, respectively.[30] As illustrated in Figure S5, the cell viability of MCF-7 and HeLa cells thoroughly reached 90% when the concentrations of chlorpromazine, amiloride, nocodazole, and genistein were 4, 100, 0.5, and 60 μg/mL, respectively.

The quantitative internalization and uptake efficiency of DOX@MSNs-COS-CMC were measured by flow cytometry analysis (Figure 3). The uptake efficiency decreased to 70%, 41%, 35%, and 63% when MCF-7 cells were pretreated with chlorpromazine, amiloride, nocodazole, and genistein, respectively. Meanwhile, the uptake efficiency decreased to 41%, 47%, 79%, and 90% when HeLa cells were pretreated with the above corresponding inhibitors, respectively. The results reveal that the uptake mechanisms of DOX@MSNs-COS-CMC are, respectively, macropinocytosis and vesicular transport for MCF-7 cells and clathrin-mediated endocytosis and macropinocytosis for HeLa cells. Clathrin-mediated endocytosis and

https://dx.doi.org/10.1021/acs.molpharmaceut.0c00004
Mol. Pharmaceutics XXXX, XXX, XXX−XXX

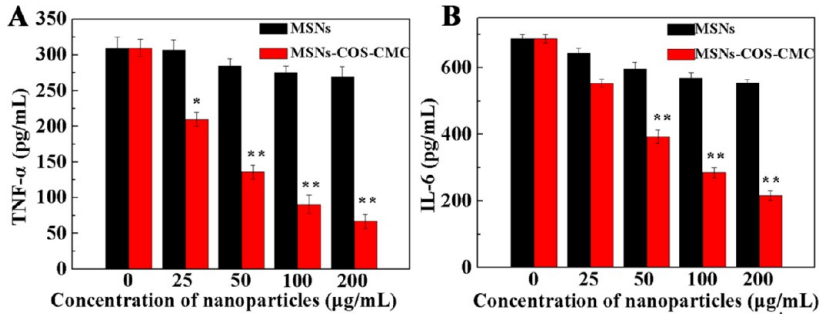

Figure 5. Inhibitory effect of blank nanoparticles on proinflammatory cytokines/chemokines in HeLa cells. The secretion of TNF-α (A) and IL-6 (B). Data were presented as the mean value ± standard deviation (n = 3). The statistical significance was analyzed by Student's t test and one-way ANOVA using SPSS software; * means $P < 0.05$, and ** means $P < 0.01$, compared with the LPS-induced group.

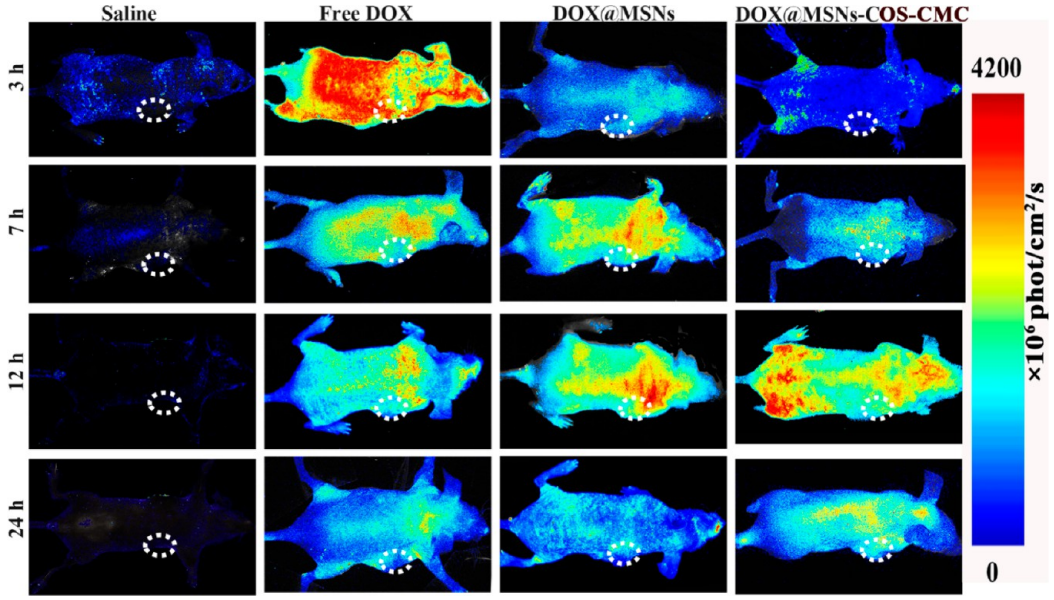

Figure 6. Time-dependent biodistribution of DOX in HeLa-bearing BALB/c-nu female mice treated with free DOX, DOX@MSNs, and DOX@MSNs-COS-CMC. (DOX dose: 5 mg/kg mouse via intravenous injection, the white circles indicate the location of the tumors).

vesicular transport played important roles in the cell type-dependent endocytosis of charge-reversible DOX@MSNs-COS-CMC.

3.4. Intracellular Tracking in HeLa cells. The endosomal escape of DOX-loaded nanoparticles in HeLa cells was further investigated by confocal microscopy. Hoechst and LysoTracker Green were used to label the nucleus and lysosome, respectively. The fluorescence intensity and localization of DOX could be clearly observed in the pixel intensity profiles (right panel of Figure 4, Figures S6 and S7). As illustrated in Figure 4, DOX fluorescence of DOX@MSNs-COS-CMC almost colocalized with LysoTracker Green-labeled lysosomes after 1 h. However, DOX gradually translocated from the lysosome to the cytoplasm, and a small amount of DOX accumulated into the nucleus after 3 h. Moreover, DOX fluorescence in the nucleus significantly increased when the incubation time was prolonged to 8 h. Compared with DOX@MSNs-COS-CMC, free DOX and DOX@MSNs colocalized with nucleus and lysosomes, respectively (Figures S6 and S7). Pearson's correlation coefficient value (Rr)[13] was calculated from CLSM images using ImageJ software (Figure S8). It should be noticed that the colocalization of DOX@MSNs-COS-CMC and lysosome/endosome was significantly decreased from 0.61 to 0.25 after 8 h, indicating a good endosomal escape ability. Theoretically, the phenomenon was attributed to the proton sponge effects of the amino groups in DOX@MSNs-COS-CMC.

3.5. Anti-Inflammatory Effects in HeLa cells. The concentrations of tumor necrosis factor-alpha (TNF-α) and interleukin 6 (IL-6) were evaluated using the ELISA assay, in order to confirm the anti-inflammatory effects of MSNs-COS-CMC and DOX@MSNs-COS-CMC on lipopolysaccharide (LPS)-induced HeLa cells (Figure 5 and Figure S9). Although the cell viability of HeLa was not reduced after the treatment of MSNs-COS-CMC at 25 and 200 μg/mL, the IL-6 concentration decreased by 20% and 70%, and the TNF-α level decreased by 32% and 80% when HeLa cells were treated with MSNs-COS-CMC at the corresponding concentration. Results demonstrated that MSNs-COS-CMC exhibited significant anti-inflammatory activity in a dose-dependent manner.

The levels of TNF-α and IL-6 were markedly increased in the free DOX group. However, secretions of TNF-α and IL-6 were alleviated in the DOX@MSNs-COS-CMC group. The above results suggested that the anti-inflammatory activity of MSNs-COS-CMC could be attributed to the COS-CMC shell.

3.6. In Vivo Fluorescence Imaging and Biodistribution in Tumor-Bearing Mice. The biodistribution of DOX

https://dx.doi.org/10.1021/acs.molpharmaceut.0c00004
Mol. Pharmaceutics XXXX, XXX, XXX−XXX

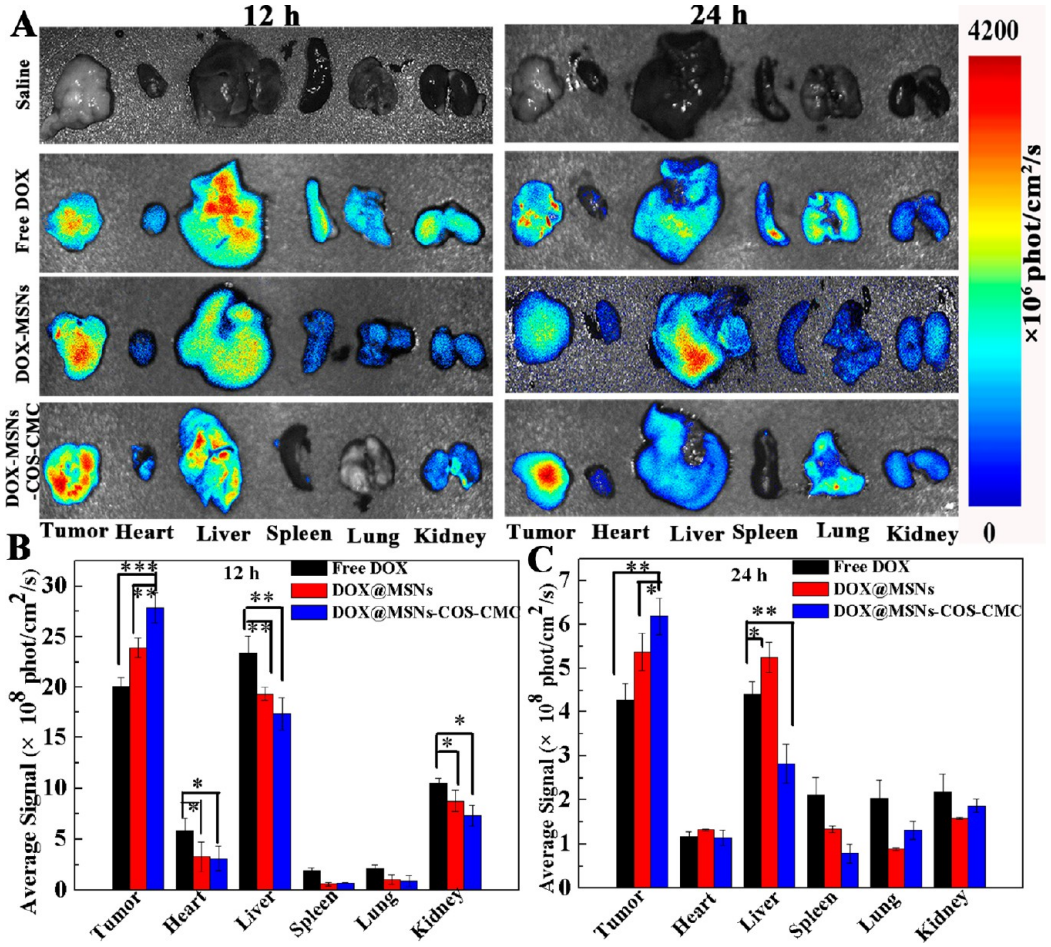

Figure 7. Fluorescence intensity analysis of extracted tumors and organs. (A) Ex vivo images of tumors and organs. The histogram shows the DOX signal in tumors calculated from the in vivo fluorescence imaging. (B, C) Semiquantitative fluorescence intensity at 12 and 24 h postinjection. Data were presented as the mean value ± standard deviation (n = 3); the statistical significance was analyzed by Student's t test and one-way ANOVA using SPSS software, * means $P < 0.05$, and ** means $P < 0.01$.

in HeLa tumor-bearing nude mice was investigated to determine the targeting capability of DOX-loaded nanoparticles during blood circulation by the in vivo fluorescence imaging system. As shown in Figure 6, DOX fluorescence signals were rapidly decreased in the free DOX groups after 3 h, due to the short blood half-life and rapid elimination in vivo.[37] The DOX fluorescence signals of DOX@MSNs-COS-CMC were slightly increased over time and reached the maximum at the time point of 12 h, owing to the enhanced permeability and retention effect.[38,39] The results indicate that DOX@MSNs-COS-CMC exhibit long circulation capability and good tumor-targeting capacity.

The main organs and tumor tissues were harvested to evaluate the ex vivo DOX fluorescence intensity at 12 and 24 h postinjection (Figure 7A–C). DOX fluorescence was substantially accumulated in the heart, liver, and kidneys, but slightly distributed in the tumor tissue due to the nontargeting effects of free DOX, while DOX accumulations in tumor tissues were apparently increased in the DOX@MSNs-COS-CMC group due to the prevention of premature drug release and the enhanced tumor-targeting activity (Figure 7B,C). The results are in accordance with the in vivo animal imaging results, which is ascribed to the endocytosis of drug-loaded nanoparticles to facilitate the deep tumor penetration and cell apoptosis at the tumor site.[39,40] The data suggest that DOX@MSNs-COS-CMC have an excellent targeting ability to increase tumor accumulation, which is beneficial to enhance the therapeutic efficacy in vivo.

3.7. In Vivo Anti-Tumor Effect of DOX@MSNs-COS-CMC. In vivo therapeutic efficacy of DOX-loaded nanoparticles was evaluated in HeLa-bearing nude mice, in view of the efficient tumor accumulation and penetration in tumor tissues. All mice were sacrificed since the tumors in control groups were too large on the 15th day. The changes in body weights were recorded every day as an indirect index of general toxicity (Figure 8A). A significant decrease was observed in the mice treated with free DOX, indicating the significant systemic toxicity. The body weights in the DOX@MSNs group were slightly decreased at a later stage. There was no significant weight change in the DOX@MSNs-COS-CMC group during the whole treatment period, indicating the decreased toxicity and better biocompatibility than free DOX.

Figure 8B shows that the tumor volume was rapidly increased to 1500 mm^3 after treatment of saline, while both free DOX and DOX-loaded nanoparticles exhibited a superior suppression in tumor growth. Figure 8C shows that DOX@MSNs-COS-CMC had the highest tumor inhibition among the different groups. The tumor weight of the DOX@MSNs-COS-CMC group was approximately 0.20 g; in contrast, the tumor weights of the other groups were higher (control = 0.79 g, free

https://dx.doi.org/10.1021/acs.molpharmaceut.0c00004
Mol. Pharmaceutics XXXX, XXX, XXX−XXX

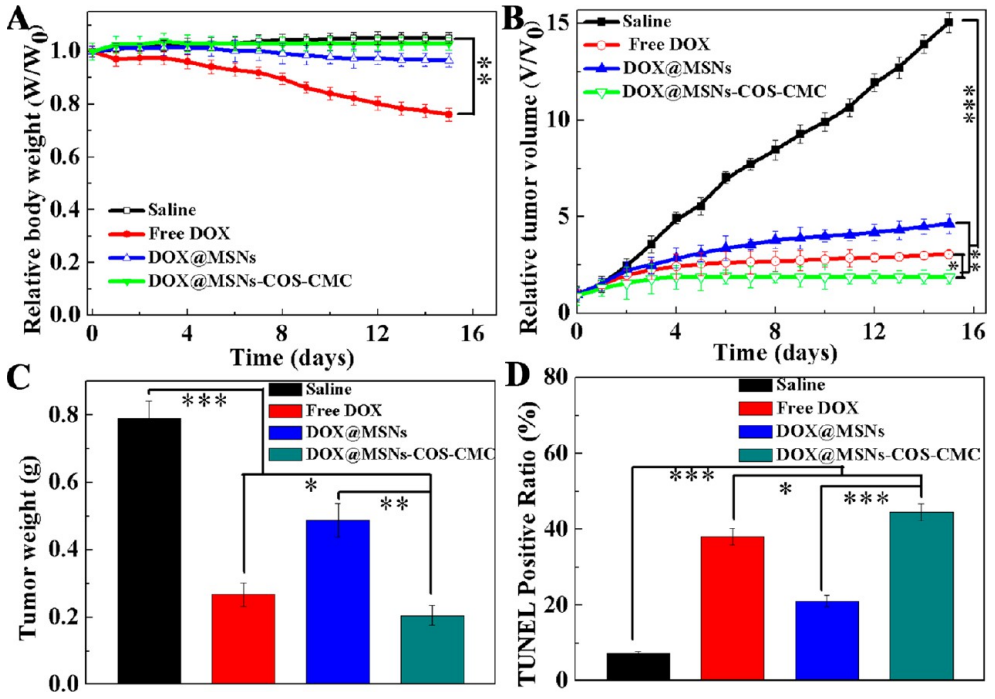

Figure 8. In vivo antitumor effects of saline, free DOX, DOX@MSNs, and DOX@MSNs-COS-CMC on HeLa tumor-bearing mice. (A) Changes in relative body weight. (B) Relative tumor volumes. (C) Weight of tumors stripped from mice after the last injection. (D) Quantitative analysis of apoptotic cells by the TUNEL staining assay. The apoptotic indices were measured as the ratio of apoptotic cells to the total tumor cells in each microscopic field view. Data were presented as the mean value ± standard deviation (n = 3). The statistical significance was analyzed by Student's t test and one-way ANOVA using SPSS software; * means $P < 0.05$, and ** means $P < 0.01$.

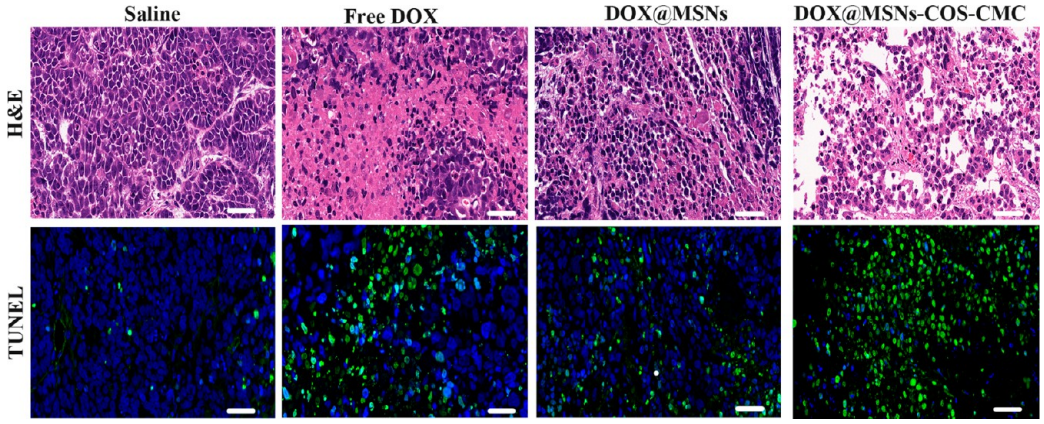

Figure 9. H&E and TUNEL staining analysis of tumors after treatment with saline, free DOX, DOX@MSNs, and DOX@MSNs-COS-CMC. Scale bars: 50 μm. In TUNEL immunofluorescence staining, the nuclei were labeled with DAPI (blue), and the apoptotic cells were green. The scale bars were 50 mm.

DOX = 0.28 g, DOX@MSNs = 0.50 g). In addition, tumors in the DOX@MSNs-COS-CMC group were smaller in size (Figure S10), indicating excellent antitumor activity.

H&E and TUNEL staining were carried out to investigate the mechanism of the antitumor efficiency of drug-loaded nanoparticles. Figure 9 shows that tumors of the saline group remained an intact physiological morphology; less apoptosis or necrosis was observed. The cancer cell swelling and vacuolization, cell nucleus shrinkage, and moderate apoptosis or necrosis were observed in free DOX and DOX@MSNs groups, whereas the maximum range of nuclei deficiency appeared in the group of DOX@MSNs-COS-CMC. Besides, similar results were found in TUNEL staining. DOX@MSNs-COS-CMC displayed the strongest apoptosis fluorescence. In addition, the quantitative analysis of apoptotic cells by the TUNEL staining assay also confirmed the above observations (Figure 8D). The tumor inhibition of DOX@MSNs-COS-CMC was 0.4 times higher than free DOX in HeLa tumor-bearing mice. Results demonstrate that DOX@MSNs-COS-CMC have good biocompatibility and excellent performance in prominent tumor growth inhibition.

The heart, liver, spleen, lung, and kidney in mice were observed and analyzed to evaluate the cytotoxicity and side effects via H&E staining analysis (Figure 10). Histopathological changes in the heart of mice were significantly observed after treatment with free DOX. For instance, the myocardial fibers were arranged irregularly and distributed unevenly, the gaps between these fibers were widened, and the cell nuclei

https://dx.doi.org/10.1021/acs.molpharmaceut.0c00004
Mol. Pharmaceutics XXXX, XXX, XXX−XXX

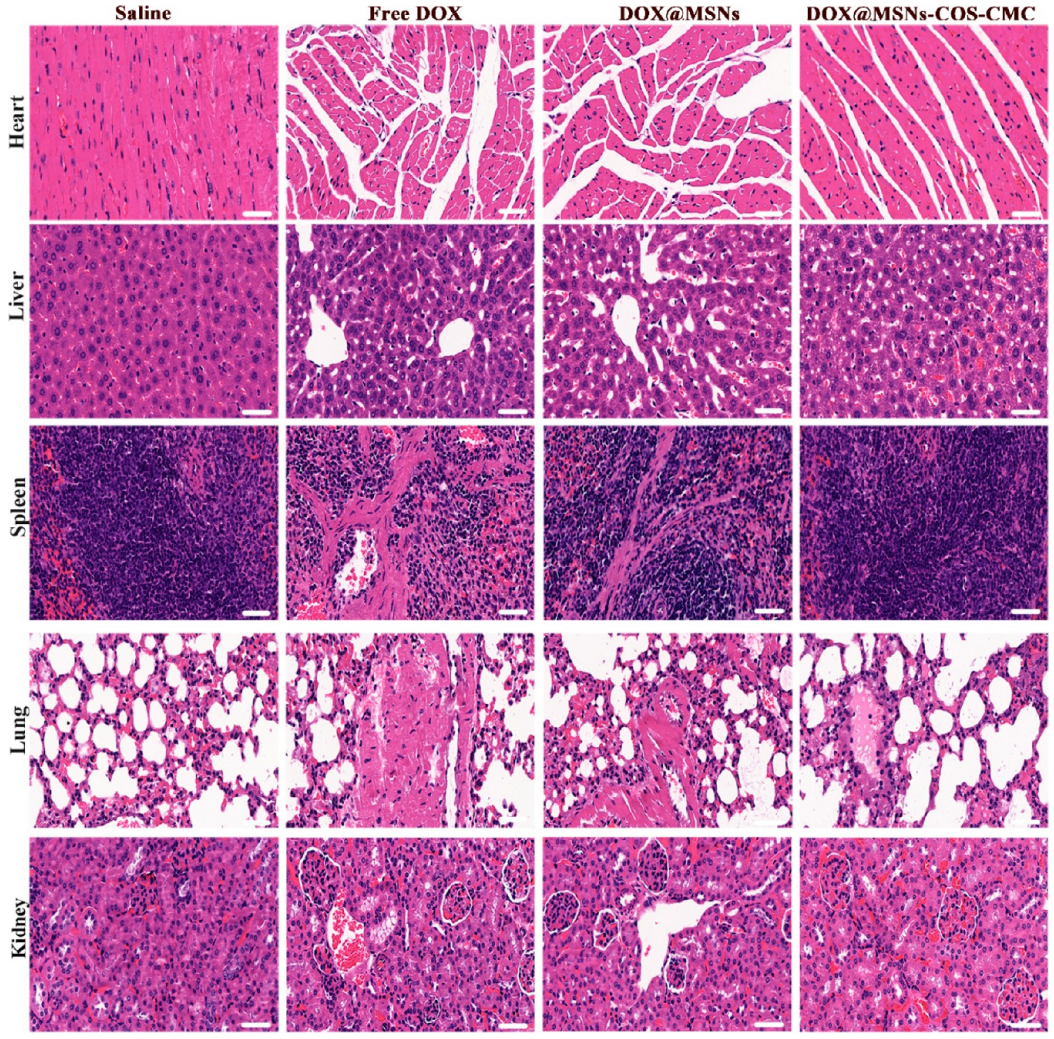

Figure 10. H&E staining analysis of the heart, liver, spleen, lung, and kidney in HeLa tumor-bearing mice after treatments with saline, free DOX, DOX@MSNs, and DOX@MSNs-COS-CMC. Scale bars: 50 μm.

was obviously deformed. Moreover, free DOX resulted in multiple organ toxicity, such as focal necrosis in the liver and acute pyogenic lesions in both the lung and spleen. However, almost no pathological changes and injuries were detected in the main tissues of the DOX@MSNs-COS-CMC group, indicating that the DOX-induced cardiotoxicity and inflammation were effectively overcome.

Results demonstrate that DOX@MSNs-COS-CMC have the synergistic targeting effects of pH sensitivity and charge reversal, providing a platform for improving the specificity, effectiveness, and safety of cancer therapy.

4. CONCLUSIONS

In summary, the charge-reversible COS-CMC shell facilitates the specificity and clathrin-mediated endocytosis to HeLa cells than MCF-7 cells at pH 6.5 and exhibits a dose-dependent anti-inflammatory activity due to the stepwise and rapid responsiveness to the tumor extracellular microenvironment. Moreover, DOX@MSNs-COS-CMC prolongs the retention time and prompts the accumulation of DOX at tumor sites. In addition, the controllable drug release further reduces the drug leakage in heart and liver tissues without compromising the therapeutic efficacy, alleviating the cardiotoxicity and inflammation in HeLa tumor-bearing mice. Thus, the cascade of cell-type specificity, endocytosis mechanism, endosomal escape, anti-inflammation, and tumor accumulation of charge-reversible DOX@MSNs-COS-CMC would provide an effective strategy for cervical carcinoma therapy.

■ ASSOCIATED CONTENT

Supporting Information

The Supporting Information is available free of charge at https://pubs.acs.org/doi/10.1021/acs.molpharmaceut.0c00004.

S/WAXS analysis, stability and drug release, kinetics fitting, cell viability, half-maximal inhibitory concentration (IC_{50}), CLSM images, in vitro cytotoxicity of pharmacological inhibitors, endosomal escape, inhibitory effects of DOX-loaded nanoparticles on the secretion of TNF-α and IL-6, and tumor images (PDF)

■ AUTHOR INFORMATION

Corresponding Authors

Wentao Liu − *School of Materials Science and Engineering, Zhengzhou University, Zhengzhou 450001, P. R. China;* orcid.org/0000-0001-8402-7486; Email: wtliu@zzu.edu.cn

https://dx.doi.org/10.1021/acs.molpharmaceut.0c00004
Mol. Pharmaceutics XXXX, XXX, XXX−XXX

Hao Liu − *School of Materials Science and Engineering, Zhengzhou University, Zhengzhou 450001, P. R. China;* orcid.org/0000-0002-7785-7075; Email: hliu@zzu.edu.cn

Chengshen Zhu − *School of Materials Science and Engineering, Zhengzhou University, Zhengzhou 450001, P. R. China;* Email: zhucs@zzu.edu.cn

Authors

Lan Cui − *School of Materials Science and Engineering, Zhengzhou University, Zhengzhou 450001, P. R. China;* orcid.org/0000-0001-5530-4528

Xiayi Feng − *State Key Laboratory of Virology, Wuhan Institute of Virology, Chinese Academy of Sciences, Wuhan 430071, P. R. China*

Qian Qin − *School of Materials Science and Engineering, Zhengzhou University, Zhengzhou 450001, P. R. China; Bio & Soft Matter, Institute of Condensed Matter and Nanosciences, Universite Catholique de Louvain, B-1348 Louvain-la-Neuve, Belgium;* orcid.org/0000-0003-3503-3286

Shuangxia Wu − *School of Materials Science and Engineering, Zhengzhou University, Zhengzhou 450001, P. R. China*

Suqin He − *School of Materials Science and Engineering and Henan Key Laboratory of Advanced Nylon Materials and Application, Zhengzhou University, Zhengzhou 450001, P. R. China*

Xinchang Pang − *School of Materials Science and Engineering, Zhengzhou University, Zhengzhou 450001, P. R. China;* orcid.org/0000-0003-2445-5221

Dong Men − *State Key Laboratory of Virology, Wuhan Institute of Virology, Chinese Academy of Sciences, Wuhan 430071, P. R. China;* orcid.org/0000-0003-1190-9570

Complete contact information is available at: https://pubs.acs.org/10.1021/acs.molpharmaceut.0c00004

Notes

The authors declare no competing financial interest.

■ ACKNOWLEDGMENTS

This work is supported by the National Natural Science Foundation of China (U1504527, 51703207 and 21803060) and Zhongyuan Science and Technology Innovation Leading Talents Project (194200510030).

■ REFERENCES

(1) Barua, S.; Mitragotri, S. Challenges associated with Penetration of Nanoparticles across Cell and Tissue Barriers: A Review of Current Status and Future Prospects. *Nano Today* **2014**, *9*, 223−243.

(2) Pei, M.; Jia, X.; Li, G.; Liu, P. Versatile Polymeric Microspheres with Tumor Microenvironment Bioreducible Degradation, pH-Activated Surface Charge Reversal, pH-Triggered "off-on" Fluorescence and Drug Release as Theranostic Nanoplatforms. *Mol. Pharmaceutics* **2019**, *16*, 227−237.

(3) Song, Y. F.; Liu, D. Z.; Cheng, Y.; Teng, Z. H.; Cui, H.; Liu, M.; Zhang, B. L.; Mei, Q. B.; Zhou, S. Y. Charge Reversible and Mitochondria/Nucleus Dual Target Lipid Hybrid Nanoparticles To Enhance Antitumor Activity of Doxorubicin. *Mol. Pharmaceutics* **2018**, *15*, 1296−1308.

(4) Xie, Y.; Qiao, H.; Su, Z.; Chen, M.; Ping, Q.; Sun, M. PEGylated carboxymethyl chitosan/calcium phosphate hybrid anionic nanoparticles mediated hTERT siRNA delivery for anticancer therapy. *Biomaterials* **2014**, *35*, 7978−7991.

(5) Yang, C.; Gao, S.; Dagnaes-Hansen, F.; Jakobsen, M.; Kjems, J. Impact of PEG Chain Length on the Physical Properties and Bioactivity of PEGylated Chitosan/siRNA Nanoparticles in Vitro and in Vivo. *ACS Appl. Mater. Interfaces* **2017**, *9*, 12203−12216.

(6) Jia, M.; Li, Y.; Yang, X.; Huang, Y.; Wu, H.; Huang, Y.; Lin, J.; Li, Y.; Hou, Z.; Zhang, Q. Development of both methotrexate and mitomycin C loaded PEGylated chitosan nanoparticles for targeted drug codelivery and synergistic anticancer effect. *ACS Appl. Mater. Interfaces* **2014**, *6*, 11413−11423.

(7) Feng, T.; Ai, X.; An, G.; Yang, P.; Zhao, Y. Charge-Convertible Carbon Dots for Imaging-Guided Drug Delivery with Enhanced in Vivo Cancer Therapeutic Efficiency. *ACS Nano* **2016**, *10*, 4410−4420.

(8) Wang, J.; Xu, M.; Cheng, X.; Kong, M.; Liu, Y.; Feng, C.; Chen, X. Positive/negative surface charge of chitosan based nanogels and its potential influence on oral insulin delivery. *Carbohydr. Polym.* **2016**, *136*, 867−874.

(9) Bae, Y. H.; Park, K. Targeted drug delivery to tumors: myths, reality and possibility. *J. Controlled Release* **2011**, *153*, 198−205.

(10) Li, L.; Raghupathi, K.; Yuan, C.; Thayumanavan, S. Surface charge generation in nanogels for activated cellular uptake at tumor-relevant pH. *Chemical Science* **2013**, *4* (9), 3654.

(11) Li, F.; Chen, W. L.; You, B. G.; Liu, Y.; Yang, S. D.; Yuan, Z. Q.; Zhu, W. J.; Li, J. Z.; Qu, C. X.; Zhou, Y. J.; Zhou, X. F.; Liu, C.; Zhang, X. N. Enhanced Cellular Internalization and On-Demand Intracellular Release of Doxorubicin by Stepwise pH-/Reduction-Responsive Nanoparticles. *ACS Appl. Mater. Interfaces* **2016**, *8*, 32146−32158.

(12) Liu, J.; Guo, X.; Luo, Z.; Zhang, J.; Li, M.; Cai, K. Hierarchically stimuli-responsive nanovectors for improved tumor penetration and programed tumor therapy. *Nanoscale* **2018**, *10*, 13737−13750.

(13) Jiang, Q.; Nie, Y.; Chen, X.; He, Y.; Yue, D.; Gu, Z. pH-Triggered Pinpointed Cascading Charge-Conversion and Redox-Controlled Gene Release Design: Modularized Fabrication for Nonviral Gene Transfection. *Adv. Funct. Mater.* **2017**, *27* (26), 1701571.1−1701571.12.

(14) Yuan, Y. Y.; Mao, C. Q.; Du, X. J.; Du, J. Z.; Wang, F.; Wang, J. Surface charge switchable nanoparticles based on zwitterionic polymer for enhanced drug delivery to tumor. *Adv. Mater.* **2012**, *24*, 5476−5480.

(15) Cui, L.; Liu, W.; Liu, H.; Qin, Q.; Wu, S.; He, S.; Pang, X.; Zhu, C.; Shen, P. pH-Triggered Charge-Reversal Mesoporous Silica Nanoparticles Stabilized by Chitosan Oligosaccharide/Carboxymethyl Chitosan Hybrids for Effective Intracellular Delivery of Doxorubicin. *ACS Applied Bio Materials* **2019**, *2*, 1907−1919.

(16) Morales, V.; Gutiérrez-Salmerón, M.; Balabasquer, M.; Ortiz-Bustos, J.; Chocarro-Calvo, A.; García-Jiménez, C.; García-Muñoz, R. A. New Drug-Structure-Directing Agent Concept: Inherent Pharmacological Activity Combined with Templating Solid and Hollow-Shell Mesostructured Silica Nanoparticles. *Adv. Funct. Mater.* **2016**, *26*, 7291−7303.

(17) Kuang, Y.; Chen, H.; Chen, Z.; Wan, L.; Liu, J.; Xu, Z.; Chen, X.; Jiang, B.; Li, C. Poly(amino acid)/ZnO/mesoporous silica nanoparticle based complex drug delivery system with a charge-reversal property for cancer therapy. *Colloids Surf., B* **2019**, *181*, 461−469.

(18) Zhang, Y.; Li, Y.; Ma, J.; Wang, X.; Yuan, Z.; Wang, W. Convenient preparation of charge-adaptive chitosan nanomedicines for extended blood circulation and accelerated endosomal escape. *Nano Res.* **2018**, *11*, 4278−4292.

(19) Mao, S.; Sun, W.; Kissel, T. Chitosan-based formulations for delivery of DNA and siRNA. *Adv. Drug Delivery Rev.* **2010**, *62*, 12−27.

(20) Li, J. L.; Cheng, Y. J.; Zhang, C.; Cheng, H.; Feng, J.; Zhuo, R. X.; Zeng, X.; Zhang, X. Z. Dual Drug Delivery System Based on Biodegradable Organosilica Core-Shell Architectures. *ACS Appl. Mater. Interfaces* **2018**, *10*, 5287−5295.

(21) Wang, F.; Sun, W.; Li, L.; Li, L.; Liu, Y.; Zhang, Z. R.; Huang, Y. Charge-Reversible Multifunctional HPMA Copolymers for Mitochondrial Targeting. *ACS Appl. Mater. Interfaces* **2017**, *9*, 27563−27574.

(22) Ho, D.; Kretzmann, J. A.; Norret, M.; Toshniwal, P.; Veder, J. P.; Jiang, H.; Guagliardo, P.; Munshi, A. M.; Chawla, R.; Evans, C. W.; Clemons, T. D.; Nguyen, M.; Kretzmann, A. L.; Blythe, A. J.; Saunders, M.; Archer, M.; Fitzgerald, M.; Keelan, J. A.; Bond, C. S.; Kilburn, M. R.; Hurley, L. H.; Smith, N. M.; Iyer, K. S. Intracellular speciation of gold nanorods alters the conformational dynamics of genomic DNA. *Nat. Nanotechnol.* **2018**, *13*, 1148−1153.
(23) Xia, Q.; Huang, J.; Feng, Q.; Chen, X.; Liu, X.; Li, X.; Zhang, T.; Xiao, S.; Li, H.; Zhong, Z.; Xiao, K. Size- and cell type-dependent cellular uptake, cytotoxicity and in vivo distribution of gold nanoparticles. *Int. J. Nanomed.* **2019**, *14*, 6957−6970.
(24) Schuster, R.; Zeindl, L.; Holzer, W.; Khumpirapang, N.; Okonogi, S.; Viernstein, H.; Mueller, M. Eulophia macrobulbon - an orchid with significant anti-inflammatory and antioxidant effect and anticancerogenic potential exerted by its root extract. *Phytomedicine* **2017**, *24*, 157−165.
(25) Lin, M. C.; Pan, C. Y.; Hui, C. F.; Chen, J. Y.; Wu, J. L. Shrimp anti-lipopolysaccharide factor (SALF), an antimicrobial peptide, inhibits proinflammatory cytokine expressions through the MAPK and NF-kappaB pathways in LPS-induced HeLa cells. *Peptides* **2013**, *40*, 42−48.
(26) Lee, J. Y.; Termsarasab, U.; Lee, M. Y.; Kim, D. H.; Lee, S. Y.; Kim, J. S.; Cho, H. J.; Kim, D. D. Chemosensitizing indomethacin-conjugated chitosan oligosaccharide nanoparticles for tumor-targeted drug delivery. *Acta Biomater.* **2017**, *57*, 262−273.
(27) Hu, D.; Xu, Z.; Hu, Z.; Hu, B.; Yang, M.; Zhu, L. pH-Triggered Charge-Reversal Silk Sericin-Based Nanoparticles for Enhanced Cellular Uptake and Doxorubicin Delivery. *ACS Sustainable Chem. Eng.* **2017**, *5*, 1638−1647.
(28) Hu, D.; Li, T.; Xu, Z.; Liu, D.; Yang, M.; Zhu, L. Self-stabilized silk sericin-based nanoparticles: In vivo biocompatibility and reduced doxorubicin-induced toxicity. *Acta Biomater.* **2018**, *74*, 385−396.
(29) Gatenby, R. A.; Gillies, R. J. Why do cancers have high aerobic glycolysis? *Nat. Rev. Cancer* **2004**, *4*, 891−899.
(30) Tian, Y.; Wu, M.; Liu, X.; Liu, Z.; Zhou, Q.; Niu, Z.; Huang, Y. Viral Nanoparticles: Probing the Endocytic Pathways of the Filamentous Bacteriophage in Live Cells Using Ratiometric pH Fluorescent Indicator. *Adv. Healthcare Mater.* **2015**, *4*, 413−419.
(31) Ma, B.; Zhuang, W.; Wang, Y.; Luo, R.; Wang, Y. pH-sensitive doxorubicin-conjugated prodrug micelles with charge-conversion for cancer therapy. *Acta Biomater.* **2018**, *70*, 186−196.
(32) Sun, Q.; Zhou, Z.; Qiu, N.; Shen, Y. Rational Design of Cancer Nanomedicine: Nanoproperty Integration and Synchronization. *Adv. Mater.* **2017**, *29*, 1606628.
(33) Zheng, Z.; Schenderlein, M.; Huang, X.; Brownbill, N. J.; Blanc, F.; Shchukin, D. Influence of Functionalization of Nanocontainers on Self-Healing Anticorrosive Coatings. *ACS Appl. Mater. Interfaces* **2015**, *7*, 22756−22766.
(34) Luo, Y.; Zhang, J.; Sun, A.; Chu, C.; Zhou, S.; Guo, J.; Chen, T.; Xu, G. Electric field induced structural color changes of SiO2@ TiO2 core−shell colloidal suspensions. *J. Mater. Chem. C* **2014**, *2*, 1990−1994.
(35) Vagvolgyi, M.; Martins, A.; Kulmany, A.; Zupko, I.; Gati, T.; Simon, A.; Toth, G.; Hunyadi, A. Nitrogen-containing ecdysteroid derivatives vs. multi-drug resistance in cancer: Preparation and antitumor activity of oximes, oxime ethers and a lactam. *Eur. J. Med. Chem.* **2018**, *144*, 730−739.
(36) Ritger, P. L.; Peppas, N. A. A simple equation for description of solute release II. Fickian and anomalous release from swellable devices. *J. Controlled Release* **1987**, *5*, 37−42.
(37) Ma, J.; Kang, K.; Zhang, Y.; Yi, Q.; Gu, Z. Detachable polyzwitterion coated ternary nanoparticles based on peptide dendritic carbon dots for efficient drug delivery in cancer therapy. *ACS Appl. Mater. Interfaces* **2018**, *10* (50), 43923−43935.
(38) Yu, P.; Yu, H.; Guo, C.; Cui, Z.; Chen, X.; Yin, Q.; Zhang, P.; Yang, X.; Cui, H.; Li, Y. Reversal of doxorubicin resistance in breast cancer by mitochondria-targeted pH-responsive micelles. *Acta Biomater.* **2015**, *14*, 115−124.
(39) Yoo, J.; Sanoj Rejinold, N.; Lee, D.; Jon, S.; Kim, Y. C. Protease-activatable cell-penetrating peptide possessing ROS-triggered phase transition for enhanced cancer therapy. *J. Controlled Release* **2017**, *264*, 89−101.
(40) Yang, H.; Wang, Q.; Huang, S.; Xiao, A.; Li, F.; Gan, L.; Yang, X. Smart pH/Redox Dual-Responsive Nanogels for On-Demand Intracellular Anticancer Drug Release. *ACS Appl. Mater. Interfaces* **2016**, *8*, 7729−7738.

https://dx.doi.org/10.1021/acs.molpharmaceut.0c00004
Mol. Pharmaceutics XXXX, XXX, XXX−XXX